23rd Australasian Fluid Mechanics Conference – 23AFMC
Sydney, Australia
4-8 December 2022
Paper No: AFMC2022-222

Buoyancy Vortex Engine CFD Modelling Using ANSYS-CFX

Khay-Wai Leong [1*], Michael MacDonald [1], John E. Cater [2] and Richard G. J. Flay [1]

[1] Department of Mechanical and Mechatronics Engineering, University of Auckland, Auckland 1010, New Zealand

[2] Department of Engineering Science, University of Auckland, Auckland 1010, New Zealand

* Email: kleo769@aucklanduni.ac.nz

Abstract

Computational Fluid Dynamics (CFD) modelling using ANSYS-CFX has been carried out to simulate a man-made buoyancy vortex station, to explore the possibility of extracting kinetic energy at the base. The small-scale vortex CFD domain consists of a 1 kW/m^2 heated floor section, with dry air directed inwards at 30^o and 60^o horizontal swirl angles relative to the radial direction, and side and top openings at 1 atm pressure. The shear stress transport (SST) turbulence model was used together with the Boussinesq approximation. Transient simulations followed by steady-state solutions without a turbine reveal a transition from a quasi-steady single to a two-cell vortex structure as the swirl angle is increased. The single-cell structure is identified by an updraft flow of above 1 m/s across the entire vortex core, whereas the two-cell structure is created from a downdraft along the core due to an adverse axial pressure gradient. A turbine with vertical blades is then added, encased in a rotating subdomain. The simulations with the turbine show that the turbine imposes a flow-straightening effect at the vortex base when stationary at the 60^o swirl setting, yet it increased vortex swirl by imparting angular momentum when turning at 0.63 rad/s at the 30^o swirl setting, while maintaining a single-cell vortex structure.

1. Introduction

Buoyancy-induced atmospheric columnar vortices are essentially a concentrated air parcel rising due to surface heating, combined with a large angular momentum generated above the surface (Sinclair 1966). While the swirl component in naturally occurring vortices such as dust devils are generated within convective circulation loops (Carroll & Ryan 1970; Hess & Spillane 1990), horizontal swirl in man-made vortices is created through vertical guide vanes positioned around a vortex station circumference (Fitzjarrald 1973; Mullen & Maxworthy 1977; Simpson 2015). The horizontal swirl angle is defined as the inverse tangent of the tangential to radial inflow velocity ratio across each vane. A single-cell vortex updraft is typically associated with a lower swirl ratio. When the tangential velocity component is increased relative to the radial counterpart, an adverse pressure gradient is created along the vertically aligned vortex core. This results in the swirling air aloft being drawn downwards at the core, creating a second vortex cell and reducing the buoyancy effect. A shear region between the core swirl downdraft and peripheral swirl updraft causes periodic flow disturbances, leading to vortex breakdown near the surface (Zhao et al. 2004; Bluestein 2005; Stull 2016).

Attempts have been made to create buoyancy vortices and harness their kinetic energy, potentially to recover low-grade waste heat (Simpson 2015; Michaud et al. 2017). So far, the man-made vortices were affected by wind shear and turbulence in the convective boundary layer (Michaud et al. 2017), or have spread due to blockage by the energy-harvesting turbine rotor itself (Simpson 2015). While the vortex behaviour under the influence of mesoscale conditions warrants its own study, this work focuses on the flow interaction between the vortex and turbine.

Hawkes et al. (2020) reported laboratory-scale experiments on a buoyancy vortex engine that included a freewheeling cylindrical wheel simulating a turbine. The vortex-generating heat was transferred via an aluminium plate at the vortex station centre. The turbine was in the form of vertical blades held together via two end plates. A cylindrical baffle was placed above the turbine to reduce the lateral movement of the vortex axis, especially when one side of the vortex chamber was opened. It was thought that the turbine blades reduced the inflow tangential velocity while increasing the radial velocity component. This led to the vortex retaining a single-cell structure rather than a two-cell structure, that would have been the result without the turbine at the 60^{o} inlet swirl angle setting. To explore the flow interaction between the vortex and a similarly-designed turbine in greater detail, computational fluid dynamics (CFD) simulations were carried out using ANSYS-CFX.

2. Methodology

2.1 Computational Domain

Simulations were carried out without and with the turbine through a cylindrical buoyancy vortex domain spanning 6 m in diameter and 12 m in height, representing a small-scale field vortex station (Figure 1). The sides of the domain are openings set at 0 Pa and 25 ^{o}C and consist of two sections. The lower 2.5 m-height opening substitutes the 2.5-m vertical guide vanes that direct the radial and tangential flow towards the vortex station axis, whereas the upper 9.5-m opening is set as an entrainment at 0 Pa. The cylindrical top section is also set as an opening with entrainment at 0 Pa and 25 ^{o}C. The turbine features 36 blades with a NACA-0012H (Sheldahl & Klimas 1981) cross section, and is encased in a rotating sub-domain, situated at ground-level in the open space at the centre of the vortex domain.

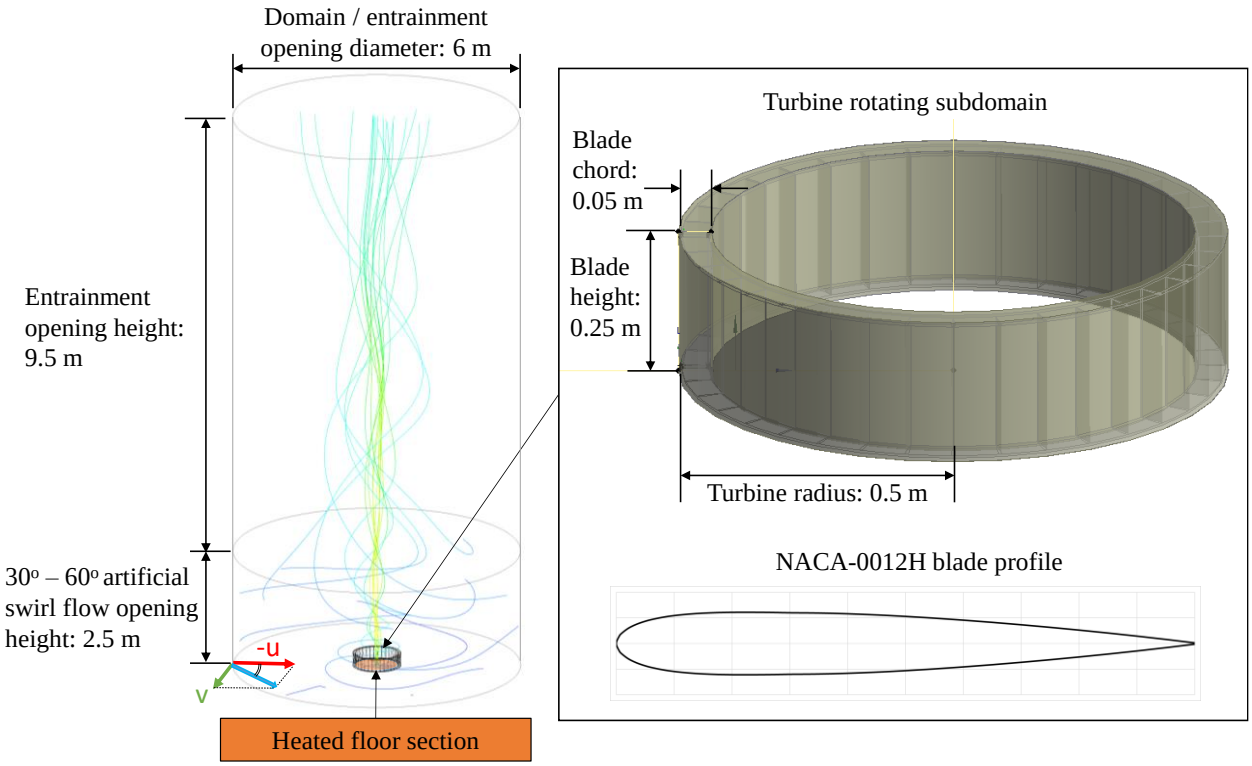

Figure 1. CFD domain of the buoyancy vortex that includes a turbine encased in a rotating mesh subdomain. The turbine features 36 vertical NACA-0012H profile blades set at 0^{o} relative to the radial direction.

Three sets of meshes, with a grid refinement index of above 1.3, were created to determine the apparent order of convergence and numerical uncertainty in the fine mesh solution, using the method described in the ASME Journal of Fluids Engineering Editorial Policy (2008). Boundary layer mesh inflation was implemented manually across the ground and heated plate sections in the stationary domain, as well as the turbine surfaces in the rotating subdomain. The rotating mesh boundaries were

set at a mere 0.005 m away from the outer turbine surfaces to mimic the actual fluid space as much as possible. However, the lack of spacing necessitated a 0.0025 m maximum inflation layer thickness across these surfaces. This resulted in a partially successful inflation layer generation, particularly for the larger mesh cells set globally across the stationary and rotating domain sections. The mesh profile details are shown in Tables 1 and 2. The inflation layer mesh thickness is taken into consideration in the subsequent vortex turbine model version.

Mesh	Global Cell Size (m)	No. of tetrahedron cells	No. of prism cells	No. of pyramid cells	Total no. of cells
N3 (Coarse)	0.119	774,886	104,205	-	879,091
N2 (Medium)	0.091	1,859,555	205,140	-	2,064,695
N1 (Fine)	0.070	4,424,543	393,630	-	4,818,173

Table 1. Vortex-only domain mesh profile.

Mesh	Global Cell Size (m)	No. of tetrahedron cells	No. of prism cells	No. of pyramid cells	Total no. of cells
N3 (Coarse)	0.098	1,307,242	174,470	17,485	1,499,197
N2 (Medium)	0.075	3,396,968	270,698	18,699	3,686,365
N1 (Fine)	0.058	8,329,460	400,925	19,644	8,750,029

Table 2. Vortex-with-turbine domain mesh profile.

Swirl flow into the domain at ground-level was artificially introduced by imposing horizontal swirl angles spanning 30^o – 60^o at the lower side opening. The CFX solver then calculated the velocity magnitudes from the buoyancy at the heat source, which is in the form of a 1 kW/m^2 heat flux emitted from a 1-m diameter wall boundary acting as a heated floor surface (located at the bottom centre of the domain). The maximum turbine speed input was determined by assuming that the maximum vortex-only tangential velocity, generated at 60^o swirl, translated fully to the maximum turbine angular velocity without any loss in angular momentum at the turbine blade leading edge. While it is acknowledged that the 1 kW/m^2 heat source is insufficient to generate a powerful vortex compared to the field experiments described in Simpson (2015) and Michaud et al. (2017), it is of interest to see the details of the initial flow development of a buoyancy vortex with and without the turbine under a minimal heat flux. The model also serves to explore the plausibility of the results generated by the CFX solver.

2.2 Numerical Methods

Given that the vortex does not form at low radial Reynolds numbers, as discovered in laboratory-scale experiments by Baker (1981), the vortex swirl flow is expected to be turbulent. The unsteady RANS equations and the k-ω based shear-stress-transport (SST) turbulence model (Menter 1994) together with the CFX automatic wall function (ANSYS 2020) were utilised, with a medium turbulence intensity (5%) boundary condition assumed. Attention was focused on the effects of buoyancy for natural convection flow, at 1 atm reference pressure and a constant 1.185 kg/m^3 air density. Given the low input heat flux and turbine speed, it was assumed that the temperature differential across both domain sections would not exceed 28 K (Gray & Giorgini 1976), so the compressibility effects on the flow field were deemed negligible, and the density was considered variable only in the gravitational term of the momentum equation. The Boussinesq approximation was therefore applied.

The High Resolution scheme (ANSYS 2020) was selected to calculate the advection terms in the continuity, momentum and energy equations, as well as the turbulence eddy frequency and kinetic

energy equations. It provides a nonlinear function to blend the central and first-order upwind differencing schemes, to minimise the effects of unphysical oscillations and of false diffusion associated with these respective differencing schemes.

The implicit second-order backward Euler time-stepping scheme was used for the transient terms in the continuity, momentum and energy equations. On the other hand, the transient terms in the turbulence model equations were calculated by deploying an implicit second-order backward Euler scheme wherever and whenever possible, reverting to a first-order backward Euler scheme when required to maintain a bounded solution (ANSYS 2020).

For the vortex-only model, a transient simulation was run at 30° swirl for 30 s, to first allow the vortex to reach a quasi-steady state of its core becoming centred along the domain axis. This was followed by a series of steady-state simulations where the inlet swirl was varied from 30° to 60° swirl over 5° increments. 10^{-4} – 10^{-6} root-mean-square residuals were reached for each steady-state simulation.

For the vortex-with-turbine model, transient (for 30 s) followed by steady-state (150 iteration) simulations were run at 30° and 60° swirl. The Coriolis and centrifugal force terms are added to the momentum equation, and the rothalpy term replaces the transient and advection terms in the total energy equation (ANSYS 2020). The Frozen Rotor frame change interface model was selected to impose a connection between the rotating and stationary frames of reference such that they each have a fixed relative position throughout the calculation. Even though the flow losses incurred between the stationary and rotating components are not simulated when the Frozen Rotor model is selected, this model uses a smaller amount of computational effort, as the quasi-steady approximation involved becomes small when the throughflow speed is large relative to the machine speed at the interface.

3. Results and Discussion

3.1 Mesh Refinement and Uncertainty Analysis

The area-averaged vorticity across a vertical cross-section of the vortex domain was used to estimate the overall vortex swirl amount. The vorticity values obtained with the 30° swirl setting and with the turbine stationary were chosen for the mesh sensitivity analysis. As shown in Figure 2, monotonic vorticity solution convergence was observed for both the vortex-only and vortex-with-turbine simulations as the meshes were refined. The apparent order of convergence for the vortex-only case was calculated to be only 0.69, with a significant 36% numerical uncertainty in the fine-grid solution. On the other hand, the apparent order of convergence for the vortex-with-turbine simulations was 2.01, with a better numerical uncertainty of 10%. This is presumably because the vortex-with-turbine domain has a finer global mesh size to start with. Still, the numerical uncertainty for the volume-averaged vertical velocity across the domain was 0.6% for the vortex-only simulations, which could give further confidence in the results obtained.

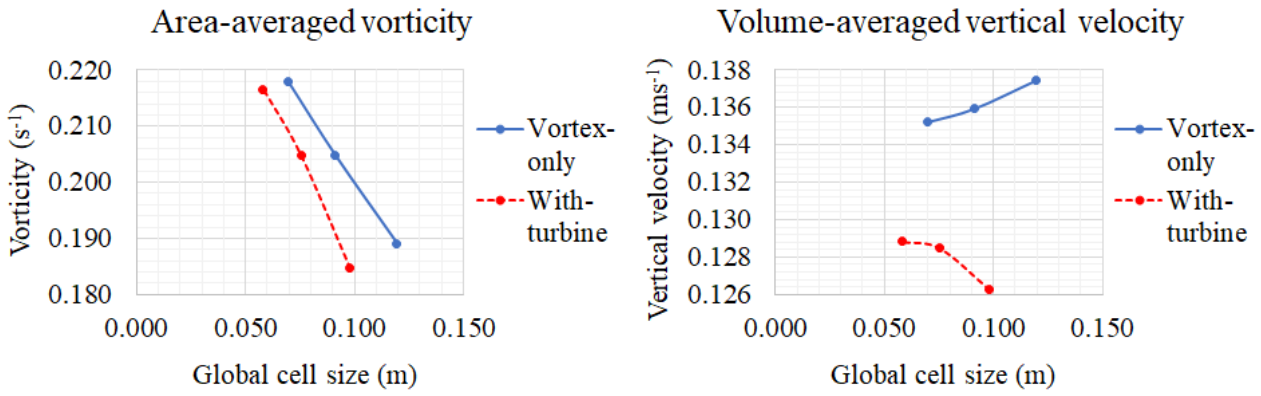

Figure 2. Area-averaged vorticity across the vortex domain vertical cross-section (left), and volume-averaged vertical velocity (right).

3.2 Effect of swirl angle and turbine on vortex structure

The vortex-only simulations reveal that when the swirl angle is at a relatively low 30°, the localised heat flux draws the air towards the centre before it rises, in a predominantly radial direction across the domain side boundaries (Figure 3). As the swirl angle is increased gradually to 45°, the increased angular momentum translates into a centrifuging effect which keeps the air from moving inwards, despite a 0.7 Pa pressure differential in the radial direction. This cyclostrophic balance has also been observed in dust devils (Sinclair 1966). At 55° and 60° swirl angles, an axial adverse pressure difference of 1.4 Pa and a distinct slow downward swirl flow (i.e., the second vortex cell) along the vortex axis are observed, causing a decrease in the area-averaged vorticity. A localised tangential velocity (indicated as Velocity v in Figure 3) increase just away from the core at ground-level is consistent with the results of dust devil large eddy simulations carried out by Zhao et al. (2004).

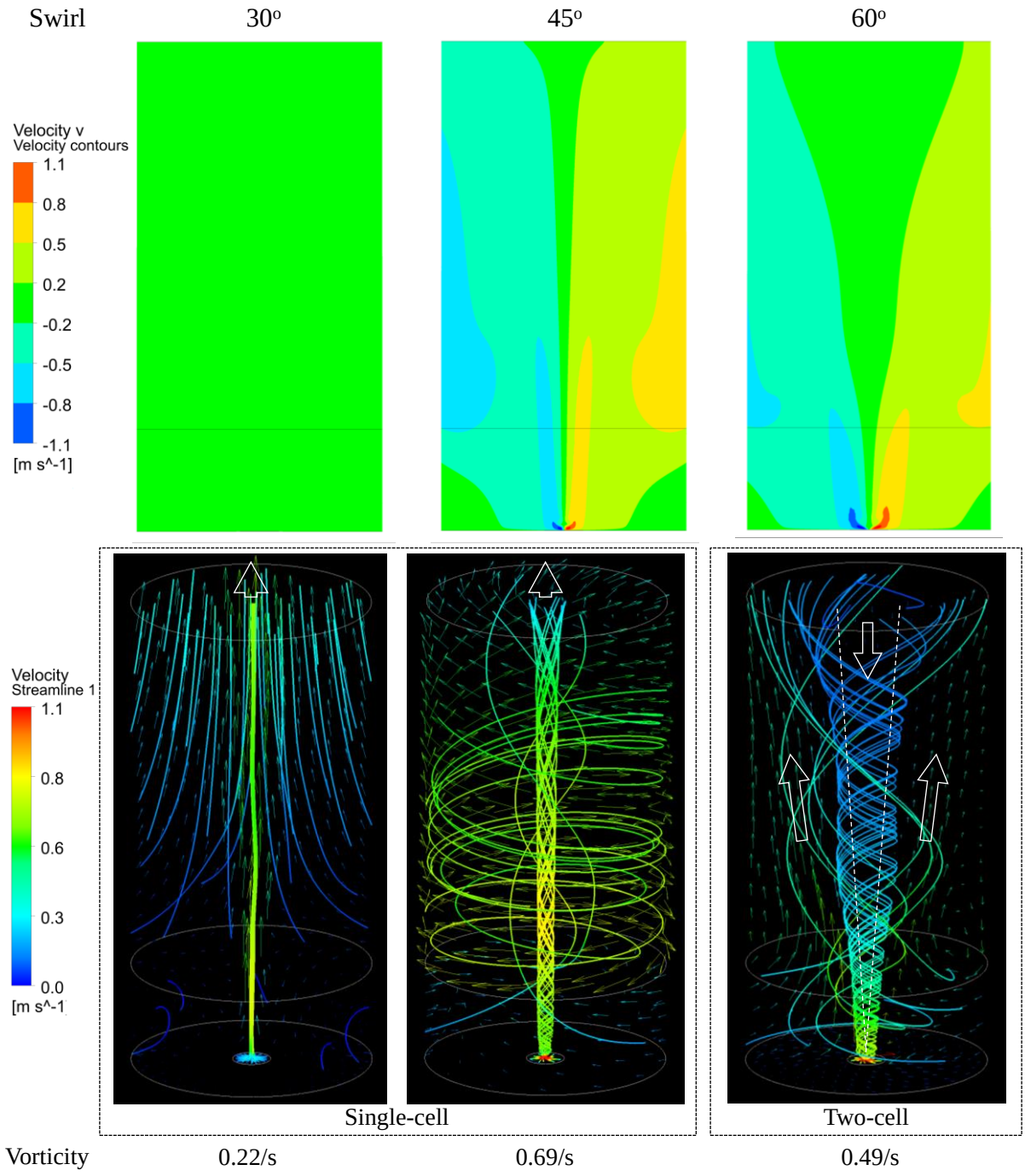

Figure 3. Vortex-only tangential velocity contours (top), streamlines and velocity vectors, as well as domain vertical plane area-average vorticity values (bottom), at 30°, 45° and 60° swirl angles.

For the vortex-with-turbine simulations, the flow fields were generated with the turbine at rest and rotating at 0.21 rad/s, 0.42 rad/s and 0.63 rad/s (Figure 4). As expected, the turbine at rest imposed a flow-straightening effect at the vortex base. The lower localised tangential velocity resulted in a reduction in the overall vorticity from 0.49/s to 0.24/s and pressure differential from 1.4 Pa to 0.1 Pa for the 60^{o} swirl setting. The reduced adverse axial pressure gradient led to the vortex retaining its single-cell updraft structure, similar to the Hawkes et al. (2020) experimental observation. On the other hand, the rotating turbine appears to act more as an impeller for the 30^{o} swirl setting, imparting an angular momentum to the incoming radial flow and increasing the vortex swirl as the flow rises and exits at the top of the domain. This can be seen in the increasing amount of helix spiral in the streamlines, shown in Figure 4, as the turbine speed is increased from 0 rad/s to 0.63 rad/s.

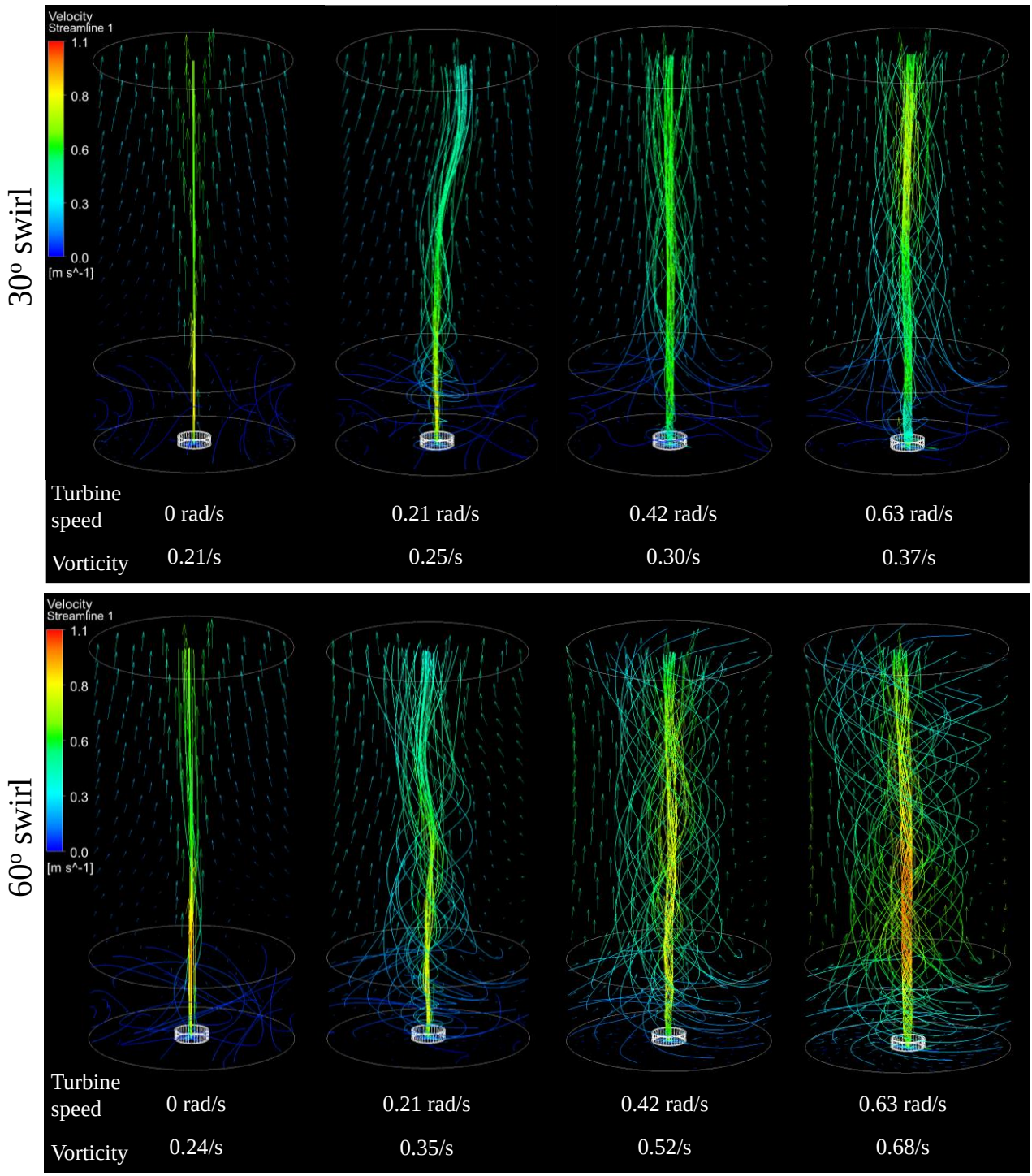

Figure 4. Vortex-with-turbine streamlines and velocity vectors, as well as domain vertical plane area-average vorticity values, at 30^{o} (top) and 60^{o} (bottom) swirl setting.

The resultant aerodynamic torque acting on the turbine fluctuated between 10^{-6} – 10^{-3} Nm without any trends for all the settings tried; this is expected given the relatively low flow velocities and turbine rotation speeds. However, it is expected that the turbine with the vertical blade design would convert the vortex kinetic energy into mechanical energy by reducing the incoming swirl angular momentum, while negating the formation of the less stable two-cell vortex structure. To further explore this hypothesis, the flow across the turbine blades will be modelled as the vortex develops under a higher heat flux, larger swirl velocities and changed boundary conditions in future.

4. Conclusions

ANSYS-CFX was used to simulate a man-made buoyancy vortex station and vortex behaviour with and without an energy-harvesting turbine at the vortex base. The vortex flow was started by imposing a small heat flux of 1 kW/m^2, using the Boussinesq approximation, and using artificial horizontal swirl angles spanning 30^o – 60^o as the initial condition. A transient followed by steady-state SST model was utilised, with a 5% turbulence intensity assumed. A mesh sensitivity analysis revealed that the vortex-only and vortex-with-turbine calculations had apparent orders of convergence of only 0.7 and 2.0 respectively. However, the vortex-only simulations demonstrated that a single-cell updraft vortex would form at swirl angles from 30^o to 50^o, whereas the higher inlet swirl inputs of 55^o and 60^o would create a two-cell vortex. This is defined by a larger pressure differential between the vortex core and peripheral region, leading to a swirl downdraft along the core and reducing the overall vorticity along the vertical plane. The turbine with its vertical blades reduced the incoming flow swirl at the 60^o swirl setting yet increased the overall vorticity at the 30^o swirl setting, helping the vortex to maintain its single-cell structure.

Acknowledgments

The authors acknowledge financial support from the Royal Society Te Apārangi of New Zealand for the Marsden Fund grant 18-UOA-013, entitled “Reap the Whirlwind and Produce Carbon-Neutral Power from Atmospheric Buoyancy Vortices”, and would like to thank Dr. Joë Pelmard for his advice in the CFD work for this project previously. Khay-Wai Leong would also like to express gratitude for the financial support from a University of Auckland Doctoral Scholarship.

References

American Society of Mechanical Engineers (ASME) 2008, Procedure for Estimation and Reporting of Uncertainty Due to Discretization in CFD Applications, *Journal of Fluids Engineering*, **130**(7), 078001.

ANSYS 2020, *ANSYS Release 2020 R1*.

Baker, G. L. 1981, *Boundary Layers in Laminar Vortex Flows*, PhD Thesis, Purdue University, USA.

Bluestein, H. B. 2005, A Review of Ground-Based, Mobile, W-Band Doppler-Radar Observations of Tornadoes and Dust Devils. *Dynamics of Atmospheres and Oceans*, **40**(3), 163-188. doi:10.1016/j.dynatmoce.2005.03.004

Carroll, J. J. & Ryan, J. A. 1970, Atmospheric Vorticity and Dust Devil Rotation, *Journal of Geophysical Research*, **75**(27), 5179-5184. doi:10.1029/JC075i027p05179

Fitzjarrald, D. E. 1973, A Laboratory Simulation of Convective Vortices. *Journal of the Atmospheric Sciences*, **30**(5), 894-902. doi:10.1175/1520-0469(1973)030

Gray, D. D. & Giorgini, A. 1976, The Validity of the Boussinesq Approximation for Liquids and Gases, *International Journal of Heat and Mass Transfer*, **19**(5), 545-551. doi:10.1016/0017-9310(76)90168-X

Hawkes, N. A., Flay, R. G. J., Cater, J. E. & MacDonald, M. 2020, Scaling of Experimental Buoyancy Vortex Structures with Respect to Power Generation, *Journal of Physics: Conference Series*, Vol. 1618, No. 3, 032008, Bristol, UK: IOP Publishing. doi:10.1088/1742-6596/1618/3/032008

Hess, G. D. & Spillane, K. T. 1990, Characteristics of Dust Devils in Australia, *Journal of Applied Meteorology and Climatology*, **29**(6), 498-507. doi:10.1175/1520-0450(1990)029

Menter, F.R. 1994, Two-Equation Eddy-Viscosity Turbulence Models for Engineering Applications, *AIAA Journal*, **32**(8), 1598-1605. doi:10.2514/3.12149

Michaud, L. M., Sheikhzadeh, M. & Ryan, K. 2017, Atmospheric Vortex Engine Prototype, retrieved 1 February 2021 from http://vortexengine.ca/Publications/AVE_LCP.pdf

Mullen, J. B. & Maxworthy, T. 1977, A Laboratory Model of Dust Devil Vortices, *Dynamics of Atmospheres and Oceans*, **1**(3), 181-214. doi:10.1016/0377-0265(77)90006-9

Sheldahl, R. E. & Klimas, P. C. 1981, Aerodynamic Characteristics of Seven Symmetrical Airfoil Sections Through 180-Degree Angle of Attack for Use in Aerodynamic Analysis of Vertical Axis Wind Turbines, *Sandia National Laboratories Energy Report SAND80-2114*.

Simpson, M. W. 2015, *Buoyancy-Induced, Columnar Vortices with Application to Power Generation*, PhD Thesis, Georgia Institute of Technology, USA.

Sinclair, P. C. 1966, *A Quantitative Analysis of the Dust Devil*, PhD Thesis, The University of Arizona, USA.

Stull, R. B. 2016, *Practical Meteorology: An Algebra-Based Survey of Atmospheric Science* (1.00b ed.), University of British Columbia, Vancouver.

Zhao, Y. Z., Gu, Z. L., Yu, Y. Z., Ge, Y., Li, Y. & Feng, X. 2004, Mechanism and Large Eddy Simulation of Dust Devils, *Atmosphere-Ocean*, **42**(1), 61-84. doi:10.3137/ao.420105